



**Titre:** Differential noncircular pulleys for cable robots and static balancing  
Title:

**Auteurs:** Dmitri Fedorov, & Lionel Birglen  
Authors:

**Date:** 2018

**Type:** Article de revue / Article

**Référence:** Fedorov, D., & Birglen, L. (2018). Differential noncircular pulleys for cable robots and static balancing. Journal of Mechanisms and Robotics, 10 (6), 1-8.  
Citation: <https://doi.org/10.1115/1.4041213>

 **Document en libre accès dans PolyPublie**  
Open Access document in PolyPublie

**URL de PolyPublie:** <https://publications.polymtl.ca/3544/>  
PolyPublie URL:

**Version:** Version finale avant publication / Accepted version  
Révisé par les pairs / Refereed

**Conditions d'utilisation:** CC BY  
Terms of Use:

 **Document publié chez l'éditeur officiel**  
Document issued by the official publisher

**Titre de la revue:** Journal of Mechanisms and Robotics (vol. 10, no. 6)  
Journal Title:

**Maison d'édition:** ASME  
Publisher:

**URL officiel:** <https://doi.org/10.1115/1.4041213>  
Official URL:

**Mention légale:** ©2018. This is the author's version of an article that appeared in Journal of Mechanisms and Robotics (vol. 10, no. 6) . The final published version is available at  
Legal notice: <https://doi.org/10.1115/1.4041213>

# Differential Noncircular Pulleys for Cable Robots and Static Balancing

**Dmitri Fedorov\***

Department of Mechanical Engineering  
Polytechnique Montréal  
Montréal, Québec, Canada  
Email: dmitri.fedorov@polymtl.ca

**Lionel Birglen**

Department of Mechanical Engineering  
Polytechnique Montréal  
Montréal, Québec, Canada  
Email: lionel.birglen@polymtl.ca

*In this paper, we introduce a mechanism consisting of a pair of noncircular pulleys with a constant-length cable. While a single noncircular pulley is generally limited to continuously winding or unwinding, the differential cable routing proposed here allows to generate non-monotonic motions at the output of the arrangement, i.e. the location of the idler pulley redirecting the cable. The equations relating its motion to rotation angles of the noncircular pulleys and to the cable length are presented in the first part of this paper. Next, we introduce a graphical method allowing us to obtain the required pulley profiles for a given output function. Our approach is finally demonstrated with two application examples: the guiding of a cable-suspended robot along a complex trajectory using a single actuator, and the static balancing of a pendulum with a 360 degree rotational range of motion.*

## 1 Introduction

Unlike with their circular counterparts, the length of cable which is wound or released during the rotation of a noncircular pulley (also referred to as a noncircular spool or a variable-radius drum) is a nonlinear function of its rotation angle and is highly sensitive to its profile. This property has been exploited in many robotic systems, for example to achieve a coordinated motion between two joints [1, 2] as an alternative to mechanical linkages, gears, or cams. One of the main advantages of using noncircular pulleys for this specific application is the reduced weight and increased distance between the joints that one can achieve. However, the most common usage of noncircular pulleys one can find in the literature so far appears to be the design of nonlinear

rotational springs for which the rotation angle vs. torque relationship is nontrivial and determined by the pulley profile [3–5]. Most noticeably, one can use this type of springs with the aim of statically balancing mechanisms, as for instance in the pioneer work presented in [6]. It is worth reminding that a statically balanced mechanism is defined as being in equilibrium for all the positions in its workspace. This property helps improving the energy efficiency of the system by restricting the actuators solely to the task of overcoming inertia and friction [7]. The use of springs instead of counterweights to achieve static balance allows to curtail the increase of the mechanism’s moments of inertia due to the addition of the balancers, as well as to keep compactness within acceptable limits. Moreover, by connecting the spring’s elongation to the winding or unwinding of a cable around a noncircular pulley, it is possible to circumvent the requirement of an ideal zero-free-length spring [8] in these balancers. In this application, noncircular pulleys have also been used to design transmission systems allowing to balance multiple-DOF serial mechanisms with as few springs as possible [9].

Another promising application of noncircular pulleys is the guiding of cable-suspended robots through a predefined trajectory. Instead of using several actuators to wind or unwind each cable connecting the end-effector to the frame of the robot, it has been proposed to couple the winding/unwinding rates of several cables and use a single actuator for this task [10, 11]. This approach shares several similarities with the use of differentials to drive cable manipulators introduced in [12, 13], although the latter work focused exclusively on circular pulleys.

For both these applications however, the noncircular pulley mechanisms presented in the literature are limited to a continuously winding (or unwinding) motion of the out-

---

\*Corresponding author

put cable. Thus, with static balancing for instance, the relationship between the spring elongation and the pulley rotation angle is restricted to a strictly increasing (or decreasing) function. In this paper, we introduce a serial cable routing for antagonistic pulleys, similar to that of the classical Weston differential [14], in which the position of an idler pulley is guided by a cable simultaneously winding on one noncircular pulley while unwinding from another. This simultaneous winding and unwinding allows to generate non-monotonic functions which can be very advantageous in both applications discussed here as will be shown. It should be noted that a pair of antagonistic springs whose elongations are guided by noncircular pulleys has previously been presented to statically balance an inverted pendulum in [15]. However, as will be shown, the use of a single constant-length cable as discussed in this paper allows for much greater angular ranges of motion and for the generation of more complex functions, including multiple stationary points.

In Section 2.1 of this paper, the kinematic analysis of a single noncircular pulley connected to an idler pulley is first carried out. In addition, Section 2.2 introduces a graphical method for the synthesis of such a non-circular pulley profile, which allows for a more intuitive design process compared with previous numerical [8] or analytical [15, 16] approaches. Next, in Section 3, the single-cable antagonistic (i.e. differential) arrangement proposed here is described and analyzed. The advantages of this configuration are then demonstrated in practice for two applications in Section 4: a cable-suspended parallel robot that is able to follow a pick-and-place trajectory while being driven by a single actuator is achieved as well as a statically balanced pendulum with a  $360^\circ$  angular range. Finally, Section 5 presents a discussion comparing the advantages and disadvantages of the proposed mechanism with respect to the current state of the art.

## 2 Single Noncircular Pulley Mechanism

### 2.1 Kinematic Analysis

As shall be detailed in this section, the behavior of a noncircular pulley can be described as the interaction, for a defined pulley profile, between three variables: the rotation angle of that pulley, the total length of the cable between its attachment point on that pulley and an exterior attachment point (or an idler pulley redirecting the cable), and the distance between the noncircular pulley and the latter point. The general geometric parameters of a single noncircular pulley are illustrated in Figure 1a. A cable, assumed inextensible, is fixed to this noncircular pulley of radius  $r = f(\theta)$  at point F, and is wound around its profile until reaching the tangent point T. Then, from points U to V, the cable is wound around an idler pulley of constant radius  $q$ . The centers of the non-circular and idler pulleys, respectively named points O and P, are located at a distance  $x$  one from the other.

While a first reference frame  $\mathcal{R}_{pulley}$  is fixed to the center of the noncircular pulley, a second frame  $\mathcal{R}_{OP}$  can be attached arbitrarily to any point on the line from O to P, with its x-axis directed towards P. The relative rotation between these two frames is measured by the angle  $\theta_p$ . The winding or unwinding of a noncircular pulley is therefore described

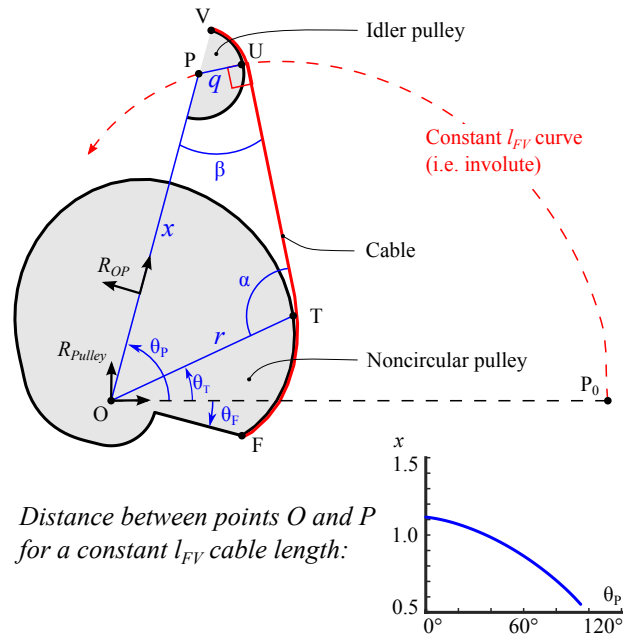


Fig. 1: Geometry of a single noncircular pulley

mathematically as:

$$g(x, \theta_p, l_{FV}) = 0, \quad (1)$$

where  $l_{FV}$  denotes the cable length from point F to point V. A similar notation is used throughout this paper for all cable lengths, i.e., the length of cable between two arbitrary points  $i$  and  $j$  is noted as  $l_{ij}$ .

The locus of the idler pulley center, i.e. all the possible locations of point P for which the cable length  $l_{FV}$  is constant, is of particular interest for the analysis performed in this paper. As plotted for the chosen example in Fig.1b, the polar equation representing this position is a strictly decreasing function  $x = f(\theta_p)$  defined by the noncircular pulley profile. It should be noted that there is an evolute-involute relationship between the profile of the noncircular pulley and the curve  $x(\theta_p)$  when the radius of the idler pulley is neglected [17].

The derivative of the latter curve, namely  $\frac{dx}{d\theta_p}$ , can be obtained by considering the differential form of the interaction between  $x$ ,  $\theta_p$ , and  $l_{FV}$ , i.e.:

$$dl_{FV} = \frac{\partial l_{FV}}{\partial \theta_p} d\theta_p + \frac{\partial l_{FV}}{\partial x} dx \quad (2)$$

and setting  $dl_{FV}$ , the infinitesimal variation of the cable length, to zero in the above equation. The assumption of a constant cable length therefore yields:

$$\frac{dx}{d\theta_p} = - \frac{\partial x}{\partial l_{FV}} \frac{\partial l_{FV}}{\partial \theta_p}. \quad (3)$$

The partial derivatives involved in Eq. (2) are highly dependent on angles  $\alpha$  and  $\beta$  shown in Fig. 1a. These angles can

be calculated for a given angle  $\theta_P$  by solving the geometric closure equations, namely:

$$q - x \sin \beta - r \sin \alpha = 0, \quad (4a)$$

$$\alpha + \beta + \theta_P - \theta_T = \pi \quad (4b)$$

where  $r$  and  $\theta_T$  are the radius and angle at the tangency point T. As established in [16], the angle  $\alpha$  is a function of the pulley profile, i.e.:

$$\sin \alpha = \frac{r}{\sqrt{\left(\frac{dr}{d\theta_T}\right)^2 + r^2}}. \quad (5)$$

Then, the total cable length  $l_{FV}$  can be expressed as  $l_{FV} = l_{FT} + l_{TU} + l_{UV}$  with:

$$l_{FT} = \int_{\theta_F}^{\theta_T} \sqrt{\left(\frac{dr}{d\theta}\right)^2 + r^2} d\theta, \quad (6a)$$

$$l_{TU} = r \cos \alpha + x \cos \beta, \quad (6b)$$

$$l_{UV} = q \left( \frac{\pi}{2} - \beta \right), \quad (6c)$$

where  $\theta_F$  is the angle corresponding to the cable attachment point on the pulley (point F). Note that Eqs (2) and (4a) to (6c) are valid whether the total cable length  $l_{FV}$  is constant or not. Taking the partial derivative of this total length  $l_{FV}$  with respect to  $\theta_P$  then yields:

$$\frac{\partial l_{FV}}{\partial \theta_P} = \frac{\partial l_{FT}}{\partial \theta_P} + \frac{\partial l_{TU}}{\partial \theta_P} + \frac{\partial l_{UV}}{\partial \theta_P} \quad (7a)$$

with:

$$\frac{\partial l_{FT}}{\partial \theta_P} = \frac{r}{\sin \alpha} \frac{d\theta_T}{d\theta_P}, \quad (7b)$$

$$\frac{\partial l_{TU}}{\partial \theta_P} = r \sin \alpha - \frac{r}{\sin \alpha} \frac{d\theta_T}{d\theta_P} + q \frac{d\beta}{d\theta_P}, \quad (7c)$$

$$\frac{\partial l_{UV}}{\partial \theta_P} = -q \frac{d\beta}{d\theta_P}. \quad (7d)$$

Thus, combining Eqs (7a) to (7c), one finally obtains:

$$\frac{\partial l_{FV}}{\partial \theta_P} = r \sin \alpha. \quad (8)$$

This partial derivative has a geometric meaning and can be interpreted as the moment arm around point O of the cable tension between points T and U assuming a constant distance  $x$ . Similarly, the partial derivative of  $l_{FV}$  with respect to  $x$  while assuming a constant rotation angle  $\theta_P$  is:

$$\frac{\partial l_{FV}}{\partial x} = \frac{\partial l_{FT}}{\partial x} + \frac{\partial l_{TU}}{\partial x} + \frac{\partial l_{UV}}{\partial x} \quad (9a)$$

$$\frac{\partial l_{FT}}{\partial x} = \frac{r}{\sin \alpha} \frac{d\theta_T}{dx}, \quad (9b)$$

$$\frac{\partial l_{TU}}{\partial x} = \cos \beta - \frac{r}{\sin \alpha} \frac{d\theta_T}{dx} + q \frac{d\beta}{dx}, \quad (9c)$$

$$\frac{\partial l_{UV}}{\partial x} = -q \frac{d\beta}{dx}, \quad (9d)$$

yielding:

$$\frac{\partial l_{FV}}{\partial x} = \cos \beta. \quad (10)$$

Equations (3), (8) and (10) can finally be combined into:

$$\frac{dx}{d\theta_P} = \frac{-r \sin \alpha}{\cos \beta}. \quad (11)$$

For a given pulley profile, given by the function  $r(\theta)$ , it is therefore possible to obtain, through integration, the relationship between  $\theta_P$  and  $l_{FV}$  assuming a constant  $x$  with Eq. (8), or between  $\theta_P$  and  $x$  assuming a constant  $l_{FV}$  with Eq. (11).

## 2.2 Graphical Synthesis

As mentioned in the previous section, the winding or unwinding of a noncircular pulley can be described as the function relating the relative angle  $\theta_P$  to  $x$ , the distance from points O to P, and the cable length  $l_{FV}$ . Three operation modes are therefore conceivable:

1. Constant  $x$ : in this mode, by far the most prevalent in the literature, the idler pulley (or the cable endpoint) is constrained to a purely rotational motion with respect to the noncircular pulley. The variation of  $l_{FV}$  during the rotation, i.e.  $\Delta l_{FV}$ , must therefore be compensated by the elongation of a spring (as in [3,5,8,15]) or by the motion of a guided body to which the cable is connected, such as the end-effector of a cable-suspended robot, see [10].
2. Constant  $l_{FV}$ : in this less frequent case, the distance  $x$  between points O and P varies. It is the common characteristic of the examples presented in this paper. The idler pulley must therefore be fixed to a moving body at the output of the system.
3. Constant  $\theta_P$ : while no example of such an arrangement has been found in the literature, it is theoretically possible and could possibly be useful to realize nonlinear springs.

In all these cases, the synthesis of the noncircular pulley profile is a problem that can be formulated as follows:

“Assuming a required relationship  $g(\theta_P, x, l_{FV}) = 0$ , what is the corresponding noncircular pulley profile defined by  $r = f(\theta)$ .”

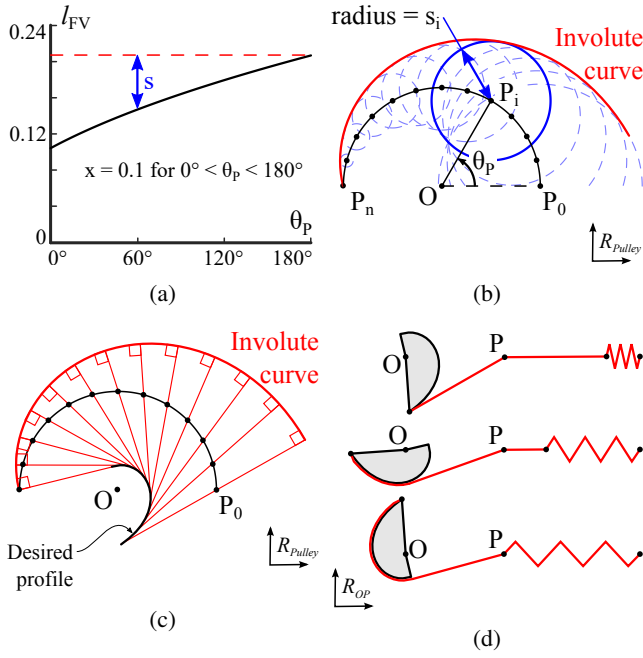


Fig. 2: Illustration of the proposed noncircular pulley synthesis method. In a) the target function  $g(\theta_P, x, l_{FV}) = 0$  is shown, in b) the involute curve is drawn, and, in c) the pulley shape is obtained from the latter curve. The rotation of the noncircular pulley in the external axes system is shown in d).

For situations where  $x$  is constant, both numerical and analytical methods have previously been used to solve this problem, e.g. in [8, 15, 16]. For the general relationship  $g(\theta_P, x, l_{FV}) = 0$ , a new graphical approach is proposed here. When  $q = 0$ , namely when the idler pulley radius is small and can be neglected or there is no idler pulley and the cable endpoint is fixed, the successive steps of the method are:

1. From the function  $g(\theta_P, x, l_{FV}) = 0$ , compute  $s(\theta_P, x, l_{FV})$  defined as the difference between  $l_{FV}$  and its maximum over the domain, as shown in Fig. 2a.
2. Discretize the functions  $g$  and  $s$  into a sequence of locations  $P_i$  of point  $P$  and associated quantities  $s_i$ , with  $i = 0, 1, \dots, n$ .
3. In the  $\mathcal{R}_{pulley}$  frame, draw a circle of radius  $s_i$  centered at  $P_i$  for each of the latter points, as illustrated in Fig. 2b. The envelope of these circles is the involute curve of the pulley profile.
4. The shape of the noncircular pulley is then defined by the envelope of the normals to the involute curve, as shown in Fig. 2c.

In the example illustrated in Fig. 2, the numerical values used correspond to the synthesis of a rotational spring having a constant torque-angle relationship, i.e.  $\tau = 1$  for  $0 < \theta_P < \pi$ . This constant torque spring is obtained by combining a noncircular pulley with a linear spring assumed to have a force-elongation relationship  $F = F_0 + ke$  where  $e$  is the spring elongation,  $k$  is its rate, and  $F_0$  is its initial tension. By using the virtual work principle, one obtains:

$$\int_0^{\theta_P} \tau(\theta) d\theta = \int_0^e F de, \quad (12)$$

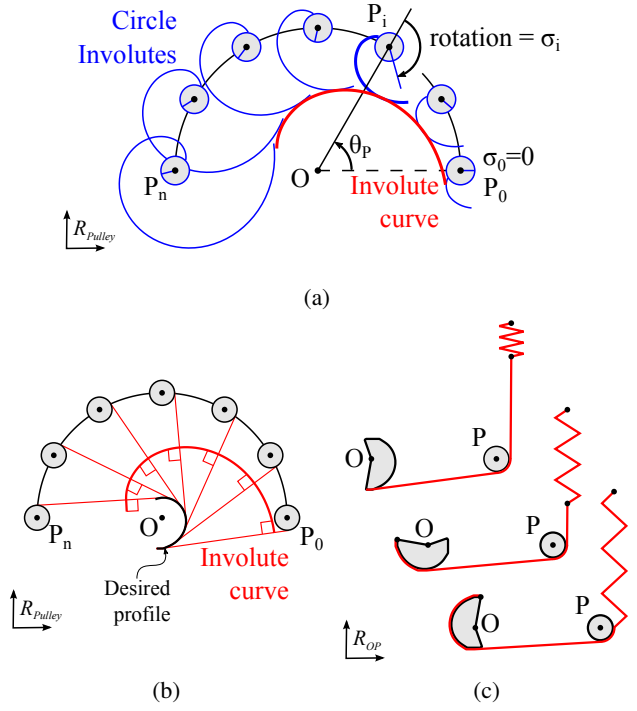


Fig. 3: Proposed synthesis method with a nonzero idler pulley radius. In a) the involute curve is drawn, and, in b) the pulley shape is obtained from the latter curve. The rotation of the noncircular pulley in the external axes system is shown in c).

which can be solved for  $e$  to yield:

$$e(\theta_P) = \frac{-F_0 + \sqrt{F_0^2 + 2k \int_0^{\theta_P} \tau(\theta) d\theta}}{k}. \quad (13)$$

This required spring elongation is realized by connecting the spring to the winding cable after it is redirected by a fixed idler pulley, which allows to write  $s(\theta_P) = \max(e(\theta_P)) - e(\theta_P)$  and  $x = \text{constant}$ . The target function  $g(\theta_P, x, l_{FV}) = 0$  thus obtained is plotted in Fig. 2a. After using the proposed graphical method (Figs. 2b-c) to generate the noncircular pulley profile, the latter is illustrated in the  $\mathcal{R}_{OP}$  frame for three values of  $\theta_P$  in Fig. 2d. Notice in this figure how, while the tension generated by the spring increases when the pulley rotates, the moment arm of the spring force decreases accordingly to keep the generated torque around  $O$  constant.

In cases where  $q \neq 0$ , the method must be adapted. At each of the successive locations  $P_i$ , one must draw the idler pulley as well as its involute curve rotated by an angle  $\sigma_i \equiv \frac{\max(s_j) - s_i}{q}$ , as illustrated in Fig. 3a. The envelope of these circle involutes is the involute of the noncircular pulley, and can be used to determine the profile of the latter (see Fig. 3b). The numerical values used for the example of Fig. 3 are identical to those of Fig. 2, with  $q = 0.02$  and  $x$  changed to 0.2 to increase readability. The resultant pulley profile is shown in the  $\mathcal{R}_{OP}$  frame for three values of  $\theta_P$  in Fig. 3c.



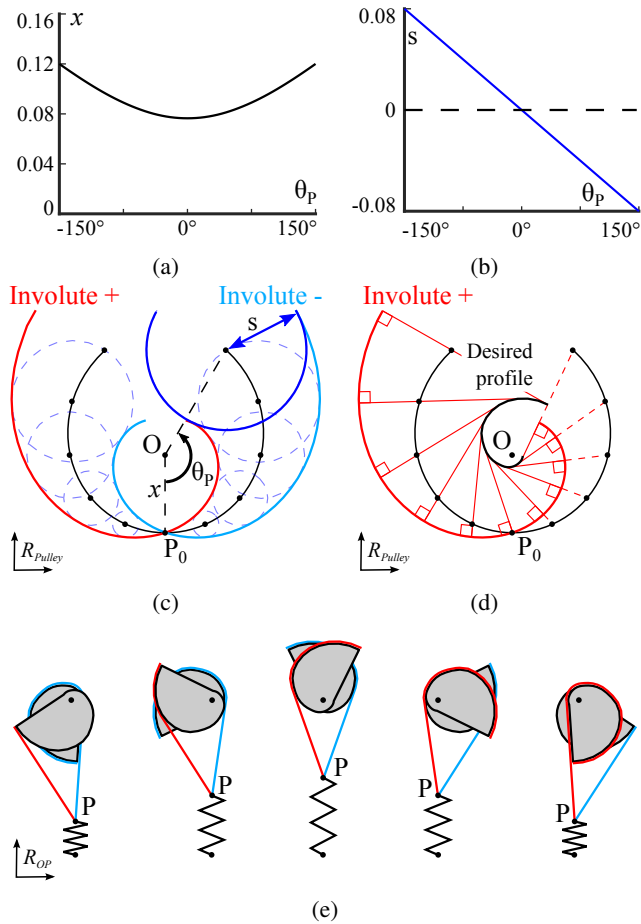


Fig. 5: Proposed synthesis method for the differential case. In a) the target distance is shown, in b) the length of cable transferred from  $l_{F+V}$  to  $l_{F-V}$  is illustrated, in c) the involute curves are drawn, and, in d) the winding pulley shape is obtained from its involute curve. The rotation of the differential pulley system in the external axes system is shown in e).

## 4 Applications

### 4.1 First Example: Cable Robot Trajectory Guiding

Several applications could benefit from the differential cable arrangement introduced in this paper. For instance, cable-suspended robots which are frequently used to move payloads through space due to their low inertia and large workspace. A common example of this technology is the SkyCam, a suspended camera often installed in stadiums [18]. Cable robots have been extensively studied, e.g. in [19–21].

The use of noncircular pulleys has been suggested for cable-suspended mechanisms in [10], where a simplified scenario consisting in the guiding of a payload supported by two cables through a horizontal linear trajectory was considered, and further developed for a two degree-of-freedom mechanism in [11]. While the length of each cable would traditionally be controlled by an independent actuator, which requires additional coordination in order to generate the desired path, the design presented in the latter references uses a single actuator driving two different pulley profiles to obtain the de-

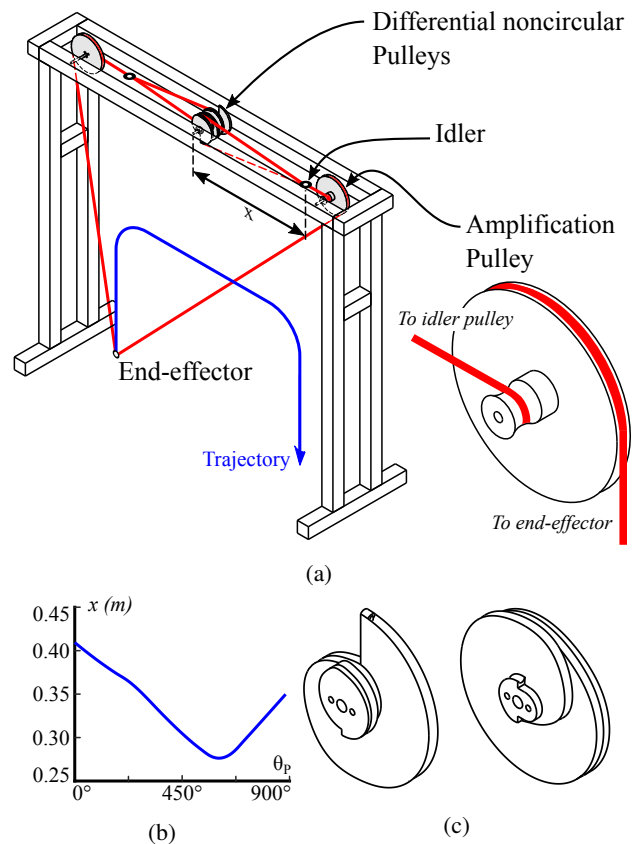


Fig. 6: Trajectory guiding for a cable-suspended robot. In a), the 3d model of the prototype is shown. In b), the target distance function is illustrated. This function can be generated using the pair of differential noncircular pulleys shown in c).

sired cable lengths corresponding to a horizontal motion at the end-effector. Altering this design to use differential cable routings for the noncircular pulleys allows to generate more complex trajectories, for which the distances between the end-effector and the attachment points of the cables vary non-monotonically. As an example, in the mechanism illustrated in Fig. 6a, the end-effector follows a pick-and-place trajectory, consisting in a sequence of upwards, horizontal, and downwards motions, a more realistic case for a practical application than solely a translation.

The motion of the end-effector consists in two vertical translations separated by an horizontal translation, with smooth transitions. The dimensions of the target trajectory are 750 mm (horizontal) per 500 mm (vertical), whereas the frame of the mechanisms is a square with 1000 mm sides. To generate the trajectory, the length of cable from the end-effector to its attachment points on the frame (near the square upper vertices) goes from 560 to 1330 mm with a non-monotonic variation. This variation is generated by connecting the end-effector cables to the motion of idler pulleys, the position of which depends on the rotation of the differential non-circular pulleys. In order to reduce the size of the mechanism, an amplification stage (shown in Fig. 6a) consisting in two coaxial pulleys with a diameter ratio of 6:1 allows to limit the idler pulley displacement to 130 mm over

an angular range set at 900 degrees, as plotted in Fig. 6b. The addition of an amplification stage does not fundamentally alter the mechanical principles behind the noncircular profile synthesis, which yields the shapes shown in Fig. 6c) through application of the graphical method described in Section 3.2.

The manufactured prototype, with ABS 3D-printed non-circular pulleys, is illustrated in Fig. 7a-b and further described in an online video: [youtu.be/13cEN7iKrMM](https://youtu.be/13cEN7iKrMM). It is driven by a RE90 Maxon motor with a 15:1 gearbox and position-controlled with an EPOS2 24/2 drive. Polyethylene fiber (Honeywell Spectra) was selected for the cable due to its high resistance and very low compliance in elongation. The end effector weighs 130 g.

The behavior of the prototype has been quantified by measuring the location of the end-effector at 45 degree intervals along the range of the input rotation. As shown in Fig. 7c-d, a relatively precise linearity has been achieved for the translations forming the trajectory. The mean deviation of the experimental coordinates from the expected trajectory is however relatively high at 9.8 mm, as the actual trajectory width, 716 mm, is significantly smaller than the expected 750 mm. However, over the total length of the trajectory, 1650 mm, this mean deviation amounts to 0.59%, while the maximal deviation of 21 mm amounts to 1.27%. Possible sources for the systematic error found for the position of the vertical translation parts of the trajectory include imprecise positioning of the cable attachment points, and imprecise cut of the initial cable lengths. From a theoretical point of view, the fact that non-circular pulleys are modeled as planar curves, although their physical implementation is a three-dimensional spiral, also leads to errors for high pulley rotation angles, as previously documented for a similar design in [10].

## 4.2 Second Example: Static Balancing of a Pendulum

Although noncircular pulleys are often used for static balancing applications [6, 8, 15], the allowable range of motion is often limited due to the strictly increasing spring elongations. Conceptually, a mass  $m$  fixed at the extremity of a pendulum of length  $l_p$  rotating in a direction perpendicular to the gravitational acceleration field is said to be statically balanced if an external system provides a torque  $\tau$  perfectly compensating the gravitational torque acting on the mass, namely:

$$\tau = mgl_p \sin \phi, \quad (15)$$

where  $g$  is the gravitational acceleration and  $\phi$  is the angle of the pendulum with respect to its stable equilibrium position. It is also possible and often more elegant to define static balancing in terms of energy, i.e. the pendulum with its mass is balanced if and only if the sum of its gravitational energy  $U_{grav}$  with the energy provided by a storage element  $U_{ext}$  is constant (see Fig. 8a). When this external element is

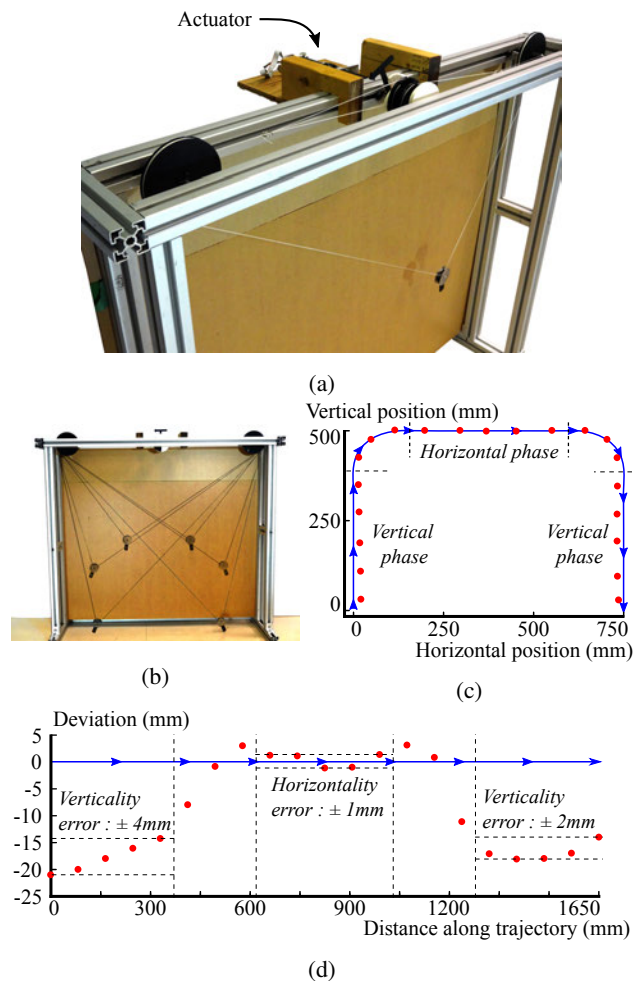


Fig. 7: Experimental results for the trajectory guiding robot. In a), an overall view of the prototype is provided, with a composite photograph of its motion shown in b). Position measurements (in blue), are superimposed on the expected trajectory (in red) in c). In d), the trajectory is unfolded to show the experimental deviations.

a spring, this condition becomes:

$$\underbrace{mgl_p(1 - \cos \phi)}_{U_{grav}} + \underbrace{F_0 e + \frac{1}{2}ke^2}_{U_{ext}} = \text{constant} \quad (16)$$

where  $e$  is the spring elongation,  $k$  is its rate, and  $F_0$  is its initial tension. Thus, in the case where the spring elongation is 0 at the unstable equilibrium position (c.f. Fig. 8a), Eq. (16) becomes:

$$mgl_p(1 - \cos \phi) + F_0 e + \frac{1}{2}ke^2 = 2mgl_p, \quad (17)$$

and the required elongation is:

$$e(\phi) = \frac{-F_0 + \sqrt{F_0^2 + 2kmgl_p(\cos \phi + 1)}}{k}. \quad (18)$$



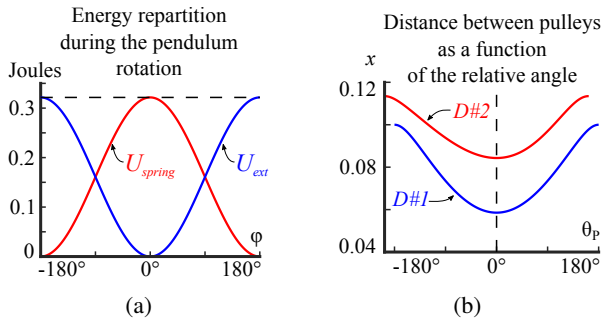


Fig. 8: Static balancing of a pendulum. In a), the constant total energy is shown for  $-\pi < \phi < \pi$ . In b), the target distance function is illustrated for both considered designs.

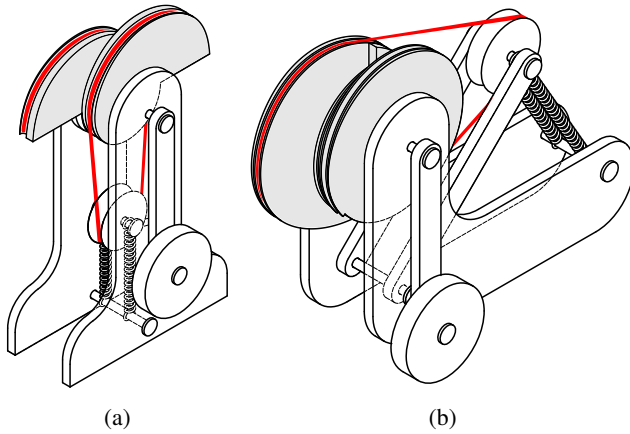


Fig. 9: Two implementations of a static balancing mechanism. In a), the motion of the idler pulley is a translation (Design #1), while in b) it is a rotation (Design #2).

The generation of the desired function  $e(\phi)$  can be achieved using the antagonistic noncircular pulleys with a differential cable routing discussed in this paper by expressing  $x$  as  $x = x_0 - e$  where the initial distance between the noncircular and idler pulleys  $x_0$  is a design parameter. If the motion of the idler pulley is purely radial with respect to the noncircular pulleys in the  $\mathcal{R}_{ref}$  reference frame, it is possible to directly equal the pendulum rotation  $\phi$  with the relative pulley angle  $\theta_p$ . In this case, the target function  $x(\theta_p)$ , shown in Fig. 8b, is symmetrical and can be physically generated by the design D#1 illustrated in Fig. 9a. For easier assembly, the motion of the idler pulley can also be constrained by a rotating link, as illustrated in Fig. 9b. In this case, the variation of the spring length creates an additional angular offset, which can be accounted for with simple trigonometry. In this case, however, the target function  $x(\theta_p)$ , shown in Fig. 8b with design D#2 (Fig 9b), becomes slightly asymmetric.

The two implementations of an axis-based mechanism transforming the pendulum's rotation into a reciprocating motion of the balancing spring discussed above share several similarities with the mechanism recently proposed in [22]. The latter reference uses a planetary set of noncircular gears and torsion bars to statically balance a pendulum over an

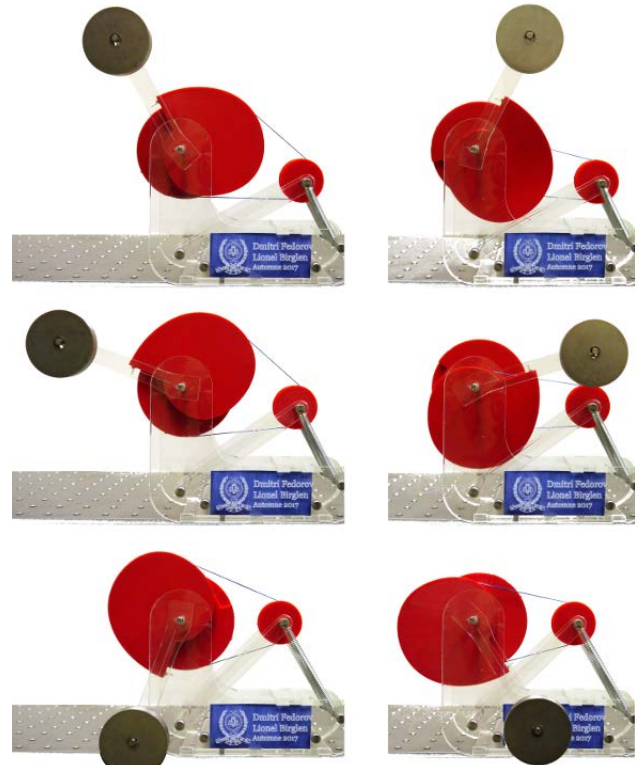


Fig. 10: Static balancing prototype shown for various pendulum angles

unlimited range of motion. This increased range however comes at the cost of more difficult machining due to the use of complex gear profiles, and increased friction due to the high number of mobile parts, as reported in that work.

Figure 10 shows a proof-of-concept prototype of the second geometry (Fig. 9b) balancing a mass of 0.17 kg fixed on a 10 cm pendulum for a  $360^\circ$  angular range, as further demonstrated in this online video : [youtu.be/yUw34IeZnIM](https://youtu.be/yUw34IeZnIM). The mechanism was manufactured using laser-cut acrylic for the frame body and links, 3d-printed ABS for the noncircular pulleys, and polyethylene fiber for the cable. The selected springs have a stiffness of  $k = 112$  N/m, with an initial preload of  $F_0 = 1.56$  N, and their elongation  $x$  varies between 0 and 41 mm over the mechanism's range of motion.

For this second prototype, performance has been evaluated by measuring the generated torque at 30 degree intervals over the angular range of the mechanism. At each position, the maximal and minimal payload weight which could be statically held (displacement smaller than  $1^\circ$  following the weight addition) were recorded. The hysteresis due to friction was then computed from this weight difference using Eq. (15) and is plotted in Fig. 11. In comparison with the nominal peak-to-peak compensated torque of 0.33 Nm, the maximal hysteresis is 0.055 Nm, which represents a relative value of 17%.

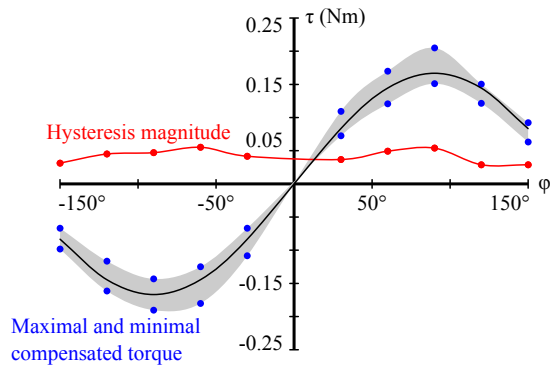


Fig. 11: Experimental results for the static balancing prototype. The minimal and maximal compensated torques are shown for various pendulum angles.

## 5 Discussion

While the trajectory guiding mechanism introduced in this paper is able to follow a more complex trajectory than previous implementations similarly using a simple rotation as input [10], it shares the main disadvantage of other one degree-of-freedom systems, namely changing this output trajectory through programming is not possible. Indeed, altering its shape, even slightly, would require replacing the noncircular pulleys driving the system. Similarly, while the cable-suspended nature of this robot allows it to have a reduced footprint, it also makes impossible to exert pushing forces beyond the effector’s weight, as the cables can only be used in tension. The maximum deviation of 1.27% is comparable in magnitude with reported relative errors of 0.79% and 0.83% for similar designs [10, 11], notably when considering the presence of an amplification stage in the mechanism introduced here, which makes small errors in the idler pulley location responsible for larger deviations at the end-effector.

In the case of the 360° static balancing mechanism, the maximal relative hysteresis of 17% is half the 36% value reported for the geared prototype described in [22], although the latter design allowed for an unlimited range of motion. In the case of noncircular pulley static balancing mechanisms, the reported maximal errors were rather 8.6% [15] and 10% [8], with angular ranges of 72° and 130° respectively. As expected, the presence of additional rotating mobile parts, whether in the form of the present prototype’s idler pulley or in that of the referenced prototype’s gears, significantly increases the effect of friction.

From a mechanical point of view, both prototypes have also demonstrated the need to carefully design the three-dimensional shape of the pulley in order to prevent the cable from slipping out of its groove. The flanges, instead of being perpendicular to the pulley axis, should be directed towards the expected location of the idler pulley, as sudden movements, for instance of the pendulum in the case of the second mechanism, can cause the cable to break loose.

Besides the applications described above, an additional contribution of the present paper lays in the introduced graphical method for noncircular pulley synthesis. In comparison with more common numerical or analytical methods,

the proposed approach implemented with a graphical user interface in `Matlab`, provides the designer with a visual tool allowing to quickly see the impact of different parameters on the pulley shape. The main advantage of this method lies in its generality and versatility as changes of the rotation angle, distance between the pulleys (both selectable through the locations  $P_i$ ), and cable length (changing the radii  $s_i$  or the angles  $\sigma_i$ ) can be arbitrarily combined. This last property is especially useful for the design of differential systems for which the distance between non-circular and idler pulleys is not constant.

## 6 Conclusion

In this paper, the capabilities of noncircular pulley (a.k.a. variable radius drum) mechanisms are expanded by introducing a differential cable routing. By simultaneously winding and unwinding the same cable from two of these pulleys, complex and previously impossible behaviors can be generated. This property was illustrated with two examples improving on common applications of noncircular pulleys, namely trajectory guiding and static balancing. Moreover, the novel graphical method for pulley profile synthesis described in this work offers an additional tool to efficiently design such mechanisms, whether differential or not.

## 7 Acknowledgements

The support of the Natural Sciences and Engineering Research Council (grant RGPIN327005) is gratefully acknowledged.

## References

- [1] Shirafuji, S., Ikemoto, S., and Hosoda, K., 2017. “Designing Noncircular Pulleys to Realize Target Motion Between Two Joints”. *IEEE/ASME Transactions on Mechatronics*, **22**(1), pp. 487–497.
- [2] Stachel, H., 2009. “Gears and Belt Drives for Non-Uniform Transmission”. *Proceedings of EUCOMES 08*, pp. 415–422.
- [3] Schmit, N., and Okada, M., 2013. “Optimal Design of Nonlinear Springs in Robot Mechanism: Simultaneous Design of Trajectory and Spring Force Profiles”. *Advanced Robotics*, **27**(1), pp. 33–46.
- [4] Shin, D., Yeh, X., and Khatib, O., 2013. “Circular Pulley Versus Variable Radius Pulley: Optimal Design Methodologies and Dynamic Characteristics Analysis”. *IEEE Transactions on Robotics*, **29**(3), pp. 766–774.
- [5] Fiorio, L., Romano, F., Parmiggiani, A., Sandini, G., and Nori, F., 2014. “Stiction Compensation in Agonist-Antagonist Variable Stiffness Actuators”. In *Proceedings of Robotics: Science and Systems*.
- [6] Ulrich, N., and Kumar, V., 1991. “Passive Mechanical Gravity Compensation for Robot Manipulators”. In *Robotics and Automation, 1991. Proceedings., 1991*

- IEEE International Conference on, IEEE, pp. 1536–1541.
- [7] Herder, J., 2001. “Energy-Free Systems: Theory, Conception, and Design of Statically Balanced Spring Mechanisms”. PhD thesis, TU Delft, Delft University of Technology.
- [8] Endo, G., Yamada, H., Yajima, A., Ogata, M., and Hirose, S., 2010. “A Passive Weight Compensation Mechanism with a Non-Circular Pulley and a Spring”. In Robotics and Automation (ICRA), 2010 IEEE International Conference on, IEEE, pp. 3843–3848.
- [9] Cui, M., Wang, S., and Li, J., 2015. “Spring Gravity Compensation Using the Noncircular Pulley and Cable For the Less-Spring Design”. In Proceedings of the 14th IFToMM World Congress, pp. 135–143.
- [10] Seriani, S., and Gallina, P., 2016. “Variable Radius Drum Mechanisms”. *Journal of Mechanisms and Robotics*, **8**(2), p. 021016.
- [11] Scalera, L., Gallina, P., Seriani, S., and Gasparetto, A., 2018. “Cable-based robotic crane (cbrc): Design and implementation of overhead traveling cranes based on variable radius drums”. *IEEE Transactions on Robotics*, **34**(2), pp. 474–485.
- [12] Khakpour, H., Birglen, L., and Tahan, S.-A., 2014. “Synthesis of Differentially Driven Planar Cable Parallel Manipulators”. *IEEE Transactions on Robotics*, **30**(3), pp. 619–630.
- [13] Khakpour, H., and Birglen, L., 2014. “Workspace Augmentation of Spatial 3-DOF Cable Parallel Robots Using Differential Actuation”. In Intelligent Robots and Systems (IROS 2014), 2014 IEEE/RSJ International Conference on, IEEE, pp. 3880–3885.
- [14] Bhavikatti, S., and Rajashekarappa, K., 1994. *Engineering Mechanics*. New Age International.
- [15] Kim, B., and Deshpande, A. D., 2014. “Design of Nonlinear Rotational Stiffness Using a Noncircular Pulley-Spring Mechanism”. *Journal of Mechanisms and Robotics*, **6**(4), p. 041009.
- [16] Schmit, N., and Okada, M., 2012. “Design and Realization of a Non-Circular Cable Spool to Synthesize a Nonlinear Rotational Spring”. *Advanced Robotics*, **26**(3-4), pp. 234–251.
- [17] Abbena, E., Salamon, S., and Gray, A., 2017. *Modern Differential Geometry of Curves and Surfaces with Mathematica*. CRC press.
- [18] Thompson, R. R., and Blackstone, M. S., 2005. Three-Dimensional Moving Camera Assembly with an Informational Cover Housing, Mar. 29. US Patent 6,873,355.
- [19] Pusey, J., Fattah, A., Agrawal, S., and Messina, E., 2004. “Design and Workspace Analysis of a 6–6 Cable-Suspended Parallel Robot”. *Mechanism and machine theory*, **39**(7), pp. 761–778.
- [20] Gouttefarde, M., and Gosselin, C. M., 2006. “Analysis of the Wrench-Closure Workspace of Planar Parallel Cable-Driven Mechanisms”. *IEEE Transactions on Robotics*, **22**(3), pp. 434–445.
- [21] Carricato, M., 2013. “Direct Geometrico-Static Problem of Underconstrained Cable-Driven Parallel Robots with Three Cables”. *Journal of Mechanisms and Robotics*, **5**(3), p. 031008.
- [22] Bijlsma, B. G., Radaelli, G., and Herder, J. L., 2017. “Design of a Compact Gravity Equilibrator with an Unlimited Range of Motion”. *Journal of Mechanisms and Robotics*, **9**(6), p. 061003.

## Listing of figure captions

Fig. 1: Geometry of a single noncircular pulley

Fig. 2: Illustration of the proposed noncircular pulley synthesis method. In a) the target function  $g(\theta_P, x, l_{FV}) = 0$  is shown, in b) the involute curve is drawn, and, in c) the pulley shape is obtained from the latter curve. The rotation of the noncircular pulley in the external axes system is shown in d)

Fig. 3: Proposed synthesis method with a nonzero idler pulley radius. In a) the involute curve is drawn, and, in b) the pulley shape is obtained from the latter curve. The rotation of the noncircular pulley in the external axes system is shown in c).

Fig. 4: Geometry of the serial cable routing for antagonistic noncircular pulleys

Fig. 5: Proposed synthesis method for the differential case. In a) the target distance is shown, in b) the length of cable transferred from  $l_{F+V}$  to  $l_{F-V}$  is illustrated, in c) the involute curves are drawn, and, in d) the winding pulley shape is obtained from its involute curve. The rotation of the differential pulley system in the external axes system is shown in e).

Fig. 6: Trajectory guiding for a cable-suspended robot. In a), the 3d model of the prototype is shown. In b), the target distance function is illustrated. This function can be generated using the pair of differential noncircular pulleys shown in c).

Fig. 7: Experimental results for the trajectory guiding robot. In a), an overall view of the prototype is provided, with a composite photograph of its motion shown in b). Position measurements (in blue), are superimposed on the expected trajectory (in red) in c). In d), the trajectory is unfolded to show the experimental deviations.

Fig. 8: Static balancing of a pendulum. In a), the constant total energy is shown for  $-\pi < \phi < \pi$ . In b), the target distance function is illustrated for both considered designs.

Fig. 9: Two implementations of a static balancing mechanism. In a), the motion of the idler pulley is a translation (Design #1), while in b) it is a rotation (Design #2).

Fig. 10: Static balancing prototype shown for various pendulum angles

Fig. 11: Experimental results for the static balancing prototype. The minimal and maximal compensated torques are shown for various pendulum angles.